# Mechanical properties of highly textured porous Ni-YSZ and Co-YSZ cermets produced from Directionally Solidified Eutectics

J.J.Roa[1,*], M. A. Laguna-Bercero[2], A. Larrea[2],V. M. Orera[2], M.Segarra[3]

[1] Institut P' (UPR 3346). Département Physique et mécanique des matériaux. CNRS-Université de Poitiers-ENSMA. Boulevard Marie et Pierre Curie SP2MI-Téléport 2-BP 30179, F-86962 Futuroscope Chasseneuil Cedex.

[2] Instituto de Ciencia de Materiales de Aragon, ICMA-Universidad de Zaragoza. Pedro Cerbuna 12, E-50009 Zaragoza (Spain).

[3] Centro DIOPMA, Universidad de Barcelona. Facultad de Quimica, Departamento de Ciencia de los Materiales e Ing. Metalurgica. Marti i Franues, 1, E-08028 Barcelona (Spain).

* Corresponding author, e-mail: jjrr_cons@hotmail.com

## Abstract

It is well known that several ceramic materials develop an usual; and sometimes unique; combination of properties as a result of mixing different phases with similar expansion coefficients. Sometimes they are elastically stiff, have relatively low thermal expansion coefficients, good thermal and electrical conductivities, and are resistant to chemical attack. As this paper will show, their mechanical properties are also enhanced.

Nanoindentation technique is used to measure the mechanical properties for each phase of NiO-YSZ and CoO-YSZ eutectics produced by the laser floating zone technique, and also the analogues Ni-YSZ and Co-YSZ cermets produced by reduction from the eutectics precursors. The different tests have been performed at a constant indentation depth of 100nm, in order to obtain a residual imprint lower than the size of the secondary phase and extract the hardness and Young's modulus using the Oliver and Pharr approach. Moreover, several tests have been

performed at 2000nm of indentation range to obtain the general response of each material. In this case, only hardness and Young's modulus of the composite can be determined. Finally, the different residual imprints have been visualized by Atomic Force Microscopy to correlate each mechanical property with each phase.

***Keywords:*** Solid Oxide Fuel Cell, Directionally Solidified eutectic, Laser floating zone technique, Ceramic materials, Nanoindentation, Hardness, Young's modulus

## 1. Introduction

Eutectic ceramic composites produced by directional solidification from melt (DSEC) are fully dense materials with a fine and homogeneous microstructure of separated phases, lamellae, fibres or more complex morphologies, well aligned along the solidification direction. They show unusual and very different properties from those expected from simple addition of the component phases [1]. The domains in directionally solidified eutectics are single crystalline which sizes ranging from hundreds of micrometers to tens of nanometers [2] connected by clean and strong interfaces at atomic scale. Moreover, the size, $\lambda$, of the eutectic structure can often be modified by simply changing the growth rate, V, according to the law $\lambda^2 V$=constant. Ceramic eutectics have been studied because of their unpaired mechanical properties consequence of the small phase size and the high quality of interfaces. Moreover, the extraordinary regularity of the eutectic microstructure and the neatness of the interfaces usually increases the thermal stability to these compounds [3]. DSEC present higher mechanical, thermal shock resistance and fracture strength than single crystals and glasses, and a better thermal stability and retention of mechanical resistance up to temperatures near to the melting point than conventional ceramic [4].

A Solid Oxide Fuel Cell (SOFC) is a device widely employed to convert the chemical energy of different types of fuel to electricity. For the anode in these devices, porous cermets of metallic nickel and yttria-stabilized cubic phase of the zirconia (YSZ) are commonly used [5,6]. The properties of these anodes are mostly dependent on their microstructure being the main concern the relatively poor mechanical properties and the tendency to coarsening of Ni particles under operation conditions. It was recently reported that highly structured porous Ni–YSZ [7] and Co-YSZ [8] produced from directionally solidified NiO/YSZ and CoO/YSZ eutectics and its subsequent reduction seem to present numerous advantages compared with conventional Ni–YSZ cermets. The stable interfaces formed between the phases during NiO-YSZ or CoO-YSZ eutectic growth and subsequent treatment of the DSE in a reducing atmosphere produces the Ni (or Co)–$ZrO_2$ cermet, where the Ni phase and the $ZrO_2$ phase are bonded by low-energy interfaces, assuring long term stability. Moreover, the channeled microstructure of this textured cermet improves the performance of the material, allowing good gas flow and electronic conduction through the Ni porous lamellae, and also provides an appropriate thermal expansion coefficient (TEC = 10.8 x $10^{-6}$ $K^{-1}$), thus achieving a good thermochemical integration with the YSZ electrolyte [9,10].

Thermo and mechanical strength are essential properties for those devices, as they are formed by various layers of different materials that have to present high-quality integration. Experimental data on the mechanical properties of DSEC are very limited because of the small size of samples available and high stiffness of the compounds involved, which implies the need of non-standard techniques to determine the strain [1]. Moreover, the component phases are not exactly “pure” single crystal phases. For example, 2 mol% $Ni^{2+}$ and 5 mol% $Co^{2+}$ ions dissolved in the YSZ matrix during the eutectic solidification process [9]. As a consequence determination of the mechanical properties of components is also of great interest.

Elastic properties of YSZ electrolytes and YSZ-NiO anode precursors were studied by Selçuk and Atkinson who obtained effective Young´s ($E_{eff}$) and shear ($G^*$) moduli using the impulse excitation technique [11]. The mechanical properties (hardness, Young's modulus and fracture toughness) of YSZ electrolytes have been previously examined by Nanoindentation technique yielding values of 19.7-14.2GPa, 260-223GPa, and 1.79MPa.$m^{1/2}$, respectively [12]. Here we have studied the mechanical properties of each component phase at nanometric scale for NiO-YSZ, Ni-YSZ, CoO-YSZ, and Co-YSZ composites. In particular, those of NiO-YSZ and CoO-YSZ eutectics produced by the laser floating zone (LFZ) technique, and also the analogues Ni-YSZ and Co-YSZ cermets produced by reduction from the eutectics precursors.

Nanoindentation is a powerful tool which allows studying the materials response at nanometric scale, by obtaining the hardness (*H*) and the Young's modulus (*E*) using the Oliver and Pharr approach. The different tests have been performed at constant penetration depths of 100nm and 2000nm, in order to either isolate the phase under study or to obtain the response of the composite, respectively.

In brittle materials indented with a Berkovich tip, surface examination of residual imprints by Atomic Force Microscopy (AFM) can reveal some typical features, such as: surface deformation effects (*sink-in* [13,14]), microcracks or damage inside the imprints [15], fracture mechanisms such as radial cracks emanating from the imprint corners [15], or *chipping* [16]. These effects may contribute to errors in the recorded depths and, consequently, to the hardness and modulus determination. We performed AFM studies of the imprints in order to ascertain that important aspect.

## 2. Experimental details

### *2.1. Samples preparation*

Precursor ceramic cylinders, 2 mm in diameter and 10 cm in length, were prepared from a mixture of the oxides NiO (99.99%, Alfa Aesar) and 8YSZ (8 mol% Y2O3-stabilized ZrO2, 99.9%, Tosoh) by cold isostatic pressing followed by sintering at 1350ºC during 12 h. Directionally solidified NiO–YSZ and CoO-YSZ eutectic rods were produced from these cylinders by the laser floating-zone method (LFZ) at a growth rate (*R*) of 100 mm/h. CoO-YSZ eutectics were growth under argon atmosphere in order to avoid CoO oxidation to $Co_3O_4$. Channeled cermets were obtained after reduction in a 5% $H_2$–Ar atmosphere at 850 ºC. Additional details about the sample preparation method, and microstructure of the cermets, as well as on the reduction kinetics process, can be found in Laguna-Bercero *et al.* [7,8,9]. The composition of the studied materials is given in Table 1.

### *2.2. Microstructural characterization*

The microstructure of the samples was studied using Optical Microscopy (OM). We have also performed transmission electron microscope (TEM Model 2000FXII, Jeol, Japan) experiments on NiO (or CoO)–YSZ and Ni (or Co)–YSZ transverse-cross sections. Ion milling (Model 600dif, Gatan, Warrendale, PA) was carried out at liquid nitrogen temperatures to prevent reduction of the YSZ phase by radiation damage.

### *2.3. Measurement of mechanical properties with a Berkovich tipped nanoindenter*

Nanoindentation tests were carried out with a Nano Indenter® XP System (Agilent Technologies) with continuous stiffness measurement, CSM (harmonic displacement 2nm and

frequency of 45Hz). The strain rate was held constant at $0.05s^{-1}$. The different experiments were performed at room temperature using a Berkovich diamond tip and performed at a maximum applied load of 100 and 2000nm. The indenter shape has been carefully calibrated for true penetration depths by indenting fused silica samples of known Young's modulus (72GPa). Surface topography around nanoindentation imprints has been observed by AFM; using a Dimension 3100 microscope from Veeco (Santa Barbara, CA) in tapping mode. Images have been then processed with the WSxM image analysis software [17].

## 3. Results and Discussion

### *3.1. Microstructure of the NiO (or CoO)-YSZ eutectics and Ni (or Co)-YSZ cermets*

NiO-YSZ and CoO-YSZ eutectic rods present regular lamellar microstructure, as observed in figure 1. Samples are formed by eutectic grains of about 10 to 80 μm. Each eutectic grain consist of NiO (or CoO) lamellae (~500 nm wide) alternating with YSZ lamellae (~400 nm wide). The major growth crystallographic directions were [100] for YSZ and ≈ [110] for NiO although growth of YSZ lamellae along the [110] directions has been also reported. At this relatively high growth rate the YSZ-CoO eutectic grows with $[111]_{CoO}$// $[111]_{YSZ}$ [9]. The low-energy interface planes have been clearly established in the YSZ-NiO eutectic as $(111)_{NiO}$//$(002)_{YSZ}$ [9]. The interlamellar spacing ($\lambda$~900 nm) is consistent with the empirical relationship $\lambda^2 R=10^{-4}$ $mm^3/h$, given by Dhalenne and Revcolevschi [18]. Subsequent treatment of the NiO-YSZ and CoO-YSZ eutectics under 5%$H_2$/Ar atmosphere at 800 ºC during 6 hours produce de resulting Ni-YSZ and Co-YSZ. Under those conditions, NiO (or CoO) is reduced to metallic Ni (or Co) forming additional porosity of 23.4 vol% and 26.2

vol% respectively. It is interesting to point out here that reduction of NiO to Ni sometimes implies a reorientation of Ni crystallographic planes [7]. Transverse cross-sections for the Ni-YSZ and Co-YSZ cermets are also shown in figure 1, where we can observe an homogeneous distribution on metal particles and pores constrained by the YSZ lamellae. These microstructure is more detailed in the TEM images shown in figure 2. Residual stresses are clearly observed for the NiO-YSZ eutectic in both NiO and YSZ phases (figure 2a), which are of about 1GPa [19]. Those residual stresses, formed after solidification due to the differences on the TEC for both components, are a clear indication of the good adhesion between phases, as the stresses have not been relaxed. As pointed before, after NiO reduction the microstructure changes to form highly porous Ni lamellae. The microstructure is now highly defective and also most of the residual stressed have been relaxed, as observed in figure 2b. Similar results were observed for the analogues CoO-YSZ and Co-YSZ samples.

### *3.2. Mechanical properties*

#### *3.2.1. Loading/unloading curve*

Loading/unloading curves have been measured in all the samples. Figure 3 displays typical loading/unloading curve for Co-YSZ. This plot supplies qualitative information about the *H* and *E* for each phase. As it can be seen, the YSZ phase presents a larger applied load than the other two different phases, then; this phase will be the hardest one. However, the porous metallic phase, *Co* in this case, will be the softest phase. In other words, the YSZ and the metal will present different deformation mechanisms; one brittle and the other one ductile, respectively. Each phase present a different deformation mechanisms under a compression tests. However, the Co-YSZ phase present an interaction of each phase, then, the mechanical

properties present a contribution of each phase. Therefore, the Young's modulus is correlated with the slope during the unloading curve. In these cases we cannot get any qualitative conclusion.

### *3.2.2. Hardness and Young's modulus*

Figure 4 and 5 exhibits the *H* and the *E* evolution, respectively from 0 to 100nm of penetration depth for each material of study and each phase. As expected, the hardness is smaller in the metallic phase. Figure 6 and 7 shows the *H* and *E* evolution for the composite at 2000nm of indentation depth. As it is shown in the Figures 5 and 7, the Young's modulus increases when the indentation depth increases until a value, which remains constant with indentation depth. Saturation values correspond to the true Young's modulus. For the low indentation depth case (100nm), the Young's modulus remains constant after 50nm depth. However, for the higher indentation depth case (2000nm), Young's modulus increases with depth until 250nm for NiO-YSZ and CoO-YSZ.

The behaviour is completely different in the case of metallic cermets. For the Ni-YSZ and Co-YSZ samples, the Young's modulus increases, reaches a maximun and then decreases with indentation depth. These phenomenon could be attributed to a relatively poor adherence between the porous metallic lamellae and the ceramic scaffold and also to the highly defective microstructure (figure 2b). This relatively bad interface will act as a microcrack between both phases and an elastic dissipation of the elastic energy could be produced yielding this instability inside of each material.

Table 2 shows the values of *H* and *E* for each phase present in the samples studied at 100 and 2000nm of maximum penetration depth.

In the case of YSZ, the data obtained by nanoindentation for *H* are higher than those reported by Dahl *et al.* [20](12.4-13.5GPa), using a Vickers microindenter, and also comparable with

the values around 16GPa reported by Menvie Bekale *et al.* [21] using microindentation. In any case, measured hardness for YSZ lamellae are in agreement with reported values of 13-20GPa [22,23,24,25] for YSZ bulk samples. However, the *H* values reported for NiO-YSZ by Roa *et al.* [25] for bulk NiO-YSZ ceramics (6.9-7.5GPa) are lower than the values obtained for NiO lamellae in this manuscript (13.8GPa). This difference could be attributed to the higher density of the eutectics (100 % dense) and also to the lamellar orientation of the component phases. As can be observe in Figure 3a, until 40nm of indentation depth exists a strong interaction between the different lamellae.

Young moduli are compared with data for the individual phases taken from literature and those calculated for the composite using the limits for isostrain (maximum) and isostress (minimum) approaches (Tables 2 and 3):

$$E= E_aV_a+E_bV_b \quad (1)$$

$$1/E=V_a/E_a+V_b/E_b \quad (2)$$

Where $E_i$ and $V_i$ are the Young modulus and volume fractions of phase a and b respectively.

The Young's modulus for NiO measured by nanoindentation is close to 220GPa given by Radovic and Lara-Curzio [27] and Giraud and Canel [26]. The E-values for the eutectic NiO-YSZ also agrees well with the value calculated for the composite. However the value obtained for CoO is smaller than that given in the literature and could be attributed to an experimental error.

In the reduced samples nanoindentation gives slightly smaller E-values for the YSZ phase than in the eutectic. The decrease in the Young modulus of the metallic phases could be due to the porosity. Effect of porosity in the effective moduli of SOFC materials has been study by Selçuk and Atkinson [11]. There are some empirical relations expressing the Young modulus as a function of porosity. The linear relationship is widely used for low porosity levels:

$$E=E_0(1-b_Ep) \quad (3)$$

here $E_0$ is the bulk Young modulus for the dense materials, p is the volume porosity and $b_E$ a fitting parameter defining the porosity dependence of the modulus. Measurements of E as a function of porosity have been done in both NiO-YSZ ceramics and Ni-YSZ cermets being $b_E$ 2.12 and 1.75 respectively [**¡Error! Marcador no definido.**]. Assuming the last value to be valid for both Ni-YSZ and Co-YSZ cermets we estimated the Young modulus of cermets in table 3.

The Young's modulus for the cermet Ni-YSZ, 110 GPa, is slightly smaller than calculated for the theoretical porosity given in Table 4 but higher that the values reported by Giraud *et al.* [26] at room temperature, 85GPa. However, Radovic and Lara-Curzio [27] report a value as small as 55GPa for a cermet with 40% of porosity and containing 63wt% of NiO before the reduction process.

As it can be seen in Table 2, the different values obtained at maximum indentation depth are in agreement with the previous values obtained at 100nm depth in the case of unreduced samples, NiO-YSZ and CoO-YSZ. These materials do not present size effect [28] because they are dense materials without internal stresses and with a good adherence between phases as corresponds to DSEC ceramics. The Young's modulus remains stable at very low indentation depths.

However, for the reduced samples the mechanical properties present strong size effect dependence. This effect could be attributed to presence of interface defects generated during the reduction process due to: *i)* different expansion coefficient between the metallic and ceramic lamella yielding a high amount of dislocations at the vicinity of the interface, *ii)* high amount of stresses generated in the interphase interface and *iii)* to internal porosity which modifies the plastic and the elastic mechanical response.

As a summary, the *E* as well as *H* of these materials; measured by nanoindentation, were higher than those reported by conventional techniques (Vickers indentation, bending, etc).

Another possibility is that by this technique we measure local mechanical properties due to the small volume of study and at that scale we only study pure phases without the influence of macroscopic defects or secondary phases.

### *3.3. Imprints visualization*

Figure 8 shows AFM images of a CoO-YSZ eutectic sample surface, cut perpendicular to the growth direction, in which indentation imprints have been performed to 100nm of indentation depth AFM reveals the presence of YSZ and CoO-lamella of about 500nm width homogeneously distributed in the textured sample. However, they cannot be easily associated to a particular eutectic component using a conventional tool like macro/microindentation technique due to the fact that the residual size of the imprint will be larger than the size of each individual phase. On the contrary, present technique allows performing indentation imprints with depths of several nanometers which allow us to isolate the mechanical behaviour of each phase. Innset 1 in Figure 8, shows a magnification of the region marked with a black square where several imprints have been performed in a YSZ grain. This is a particular experiment that allow us to unequivocally identify the properties of the YSZ phase in the case of individual YSZ lamellae.

After the mechanical characterization, the AFM observation of the different imprints permits to study the different fracture mechanisms taking place during the indentation process. As an example, Figure 9 shows different residuals imprints in a YSZ-grain in Co-YSZ samples performed at 100nm of indentation depth. As it can be seen all imprints present a field strain in the vicinity of the residual imprint. A magnification of one imprint can be observed in the inset 1. This deformation mechanism activated during the indentation process is called

chipping. In addition, this figure illustrates the presence of several cracks at the corners of the imprint due to the field stress generated during the indentation process.

Figure 10 exhibits a residual imprint performed at 2000nm of indentation depth in Co-YSZ (Figure 10a) and CoO-YSZ (Figure 10b) samples. As it can be seen, in both cases the size of the residual imprint overcomes that of lamella. At that indentation depth is impossible to isolate the contribution of each phase and only a macroscopic behaviour of each material can be obtained. Figure 10a shows an abnormal behaviour (like a kink) at the boundary of the imprint. This effect could be attributed to the ductile behaviour introduced by the metallic phase (Co). Consequently, this behaviour was not observed in CoO-YSZ sample (see fig. 10b). In that case the plastic field can be clearly observed in two sides of the imprints denoted with black arrows.

## 5.Conclusions

Nanoindentation at maximum indentation depth of 100nm and using the Oliver and Pharr approach allows us to determine the Hardness and Young's modulus for each phase present in some well-known SOFC materials: NiO-YSZ, CoO-YSZ, Ni-YSZ and Co-YSZ directionally solidified eutectics have been obtained for each phase separately. The YSZ phase is harder than the oxide (NiO and CoO) and metallic (Ni and Co) phases.

The Young's modulus and Hardness values for the interphase are in correct agreement with different values reported in the literature obtained using sharp indentations.

Nanoindentation at low indentation depth (around 100nm) allows us to isolate the mechanical properties of each phase. However, the measurements performed at 2000nm do not permit difference each phase, due to the size of the residual imprint is higher than the thickness of each phase.

## 6. Acknowledgements

We would like to thank Spanish Government and the FEDER program within the projects: MAT2008-06785-C02-01, MAT2009-14324-C02-01, GA-LC-009/2009, CEN20071018 and CIT-120000-2007-50, by the financial support and Serveis Cientificotècnics (Universidad de Barcelona) for AFM data. J.J.Roa would like to thank Dr. Emilio Jiménez-Piqué (Centre d'Integritat Estructural i Fiabilitat dels Materials, UPC) for experimental data.

## 7. References

[1] J. Llorca and V.M. Orera, "Directionally Solidified Eutectic Ceramic Oxides," *Prog. Mat. Sci.,* **51** 711-809 (2006)

[2] P.B. Oliete, J.I. Peña, A. Larrea, V.M. Orera, J. Llorca, J.Y. Pastor, A. Martín, J. Segurado, "Ultra-High-Strength Nanofibrillar $Al_2O_3$-YAG-YSZ Eutectics," *Adv. Mater.,* **19** 2313-2318 (2007)

[3] A. Sayir, S.C. Farmer, P.O. Dickerson, A.M. Yun, "High temperature mechanical properties of $Al_2O_3/ZrO_2(Y_2O_3)$ fibers," in *Mat. Res. Soc. Symp. Proc.,* **365**, 21-27 (1993)

[4] Y. Waku, N. Nakagawa, T. Wakamoto, H. Ohtsubo, K. Shimizu, Y. Kohtoku, "A ductile ceramic eutectic composite with high strength at 1873 K," *Nature,* **389** 49-52 (1997)

[5] B. C. H. Steele and A.Heinzel, ''Materials for Fuel-Cell Technologies,'' Nature, 414, 345–52 (2001).

[6] High temperature solid oxide fuel cells: fundamentals, design, and applications, Edited by Subhash C. Singhal, Kevin Kendall (2003) Elsevier.

[7] Miguel A. Laguna-Bercero, Angel Larrea, Rosa I. Merino, Jose I. Peña, and Victor M. Orera, J. Am. Ceram. Soc., 88 [11] 3215–3217 (2005)

[8] M.A. Laguna-Bercero, A. Larrea, R.I. Merino, J.I. Peña, V.M. Orera, J. Eur. Ceram. Soc. 28 (2008) 2325–2329

[9] M. A. Laguna-Bercero, A. Larrea, J.I. Peña, R. I. Merino, and V. M. Orera, ‘‘Structured Porous Ni– and Co–YSZ Solidified Eutectic Composites,’’ J. Eur. Ceram. Soc., 25, 1455–62 (2005).

[10] G. Garcia, R. I. Merino, V. M. Orera, A. Larrea, J. I. Peña, M. A. Laguna-Bercero, J. A. Pardo, J. Santiso, and A. Figueras, ‘‘YSZ Thin Films Deposited on NiO–CSZ Anodes by Pulsed Injection MOCVD for Intermediate Temperature SOFC Applications,’’ Chem. Vap. Deposition, 10, 249–52 (2004).

[11] A Selçuk and A. Atkinson, Elastic properties of ceramic oxides used in solid oxide fuel cells, J. Eur. Ceram. Soc. 17 (1997) 1523-1532

[12] M. Morales, J. J. Roa, X. G. Capdevila, M. Segarra, S. Pinol. Mechanical properties at nanometer scale of GDC and YSZ used as electrolytes for solid oxide fuel cells. *Act. Mater.*, **58**, 2504-2509 (2010).

[13] K. L. Johnson. The correlation of indentation experiments. *J. Mechan. Phys. Sol.*, **18**, 115-126 (1970).

[14] J. Alcalá, A. C. Barone, M. Anglada. The influence of plastic hardening on surface deformation modes around Vickers and spherical indents. *Acta Mater*. **48**, 3451-3464 (2000).

[15] Z. Burghard, A. Zimmermann, J. Rödel, F. Aldinger, B. R. Lawn. Crack opening profiles of indentation cracks in normal and anomalous glasses. *Acta Mater.* **52**, 293-297 (2004).

[16] B. R. Lawn, M. V. Swain, K. Phillips. On the Mode of Chipping Fracture in Brittle Solids. *J. Mater. Sci. Lett.* **10**, 1236-1239 (1975).

[17] I. Horcas, R. Fernandez, J. M. Gomez-Rodriguez, J. Colchero, J. Gomez-Herrero, and A. M. Baro. WSxM : A software for Scanning Probe Microscopy and a Tool for Nanotechnology. *Rev. Sci. Instrum.,* **78**[1] 013705, 8pp (2007).

[18] Dhalenne, G. and Revcolevschi, A., Directional solidification in the NiO–ZrO2 system. *J. Cryst. Growth*, 1984, **69**, 616–618.

[19] E. C. Dickey, V. P. Dravid, C. R. Hubbard, "Interlamellar Residual Stresses in Single Grains of NiO-$ZrO_2$(cubic) Directionally Solidified Eutectics", *J. Am. Ceram. Soc.* **80** [11], 2773-2780, (1997).

[20] P. Dahl, I. Kaus, Z. Zhao ; M. Johnson, M. Nygren, K. Wiik,T. Grade, M. –A. Einarsrud. Densification and properties of zirconia prepared by three different sintering tehcniques. *Ceram. Int.*, **33**, 1603-1610 (2007).

[21] V. Menvie Bekale, G. Sattonnay, C. Legros, A. M. Huntz, S. Poissonnet, L. Thomé. Mechanical properties of cubic zirconia irradiated with swift heavy ions. *J. Nucl. Mater*., **384**, 70-76 (2009).

[22] L. Donzel, S. G. Roberts. . *J. Eur. Ceram. Soc.*, **20**, 2457-2462 (2000).

[23] H. Jiang, Y. Lu, W. Huang, X. Li, M. Li. . *Mater. Charact.*, **51**, 1-10 (2003).

[24] S. Tekili. . *Comp. Sci/ Tech/*, **65**, 967-972 (2005).

[25] J. J. Roa, J. C. Ruiz-Morales, J. Canales-Vázquez, M. Morales, X. G. Capdevila, P. Núñez, M . Segarra. Mechanical characterization at nanometric scale of a new design of SOFCs. *Fuel Cells*, **11**, 124-130 (2011).

[26] S. Giraud, J. Canel. Young's modulus of some SOFCs materials as a function of temperature. *J. Eur. Ceram. Soc.*, **28**, 77-83 (2008).

[27] M. Radovic, E . Lara-Curzio. Elastic properties of nickel-based anodes for solid oxide fuel cells as a function of the fraction of reduced NiO. *J. Am. Ceram. Soc.*, **87**, 2242-2246 (2004).

[28] J. J. Roa, A. Magraso, M. Morales, P. Núñez, M. Segarra. Determination of hardness, young's modulus and fracture toughness of lanthanum tungstates as novel proton conductors. *Ceramics International*, **XXX**, XXX-XXX (2011).

**Figure Captions**

**Figure 1.** Optical image of the transverse cross-section of a NiO-YSZ, CoO-YSZ DSE eutectic and also for the Ni-YSZ and Co-YSZ cermets. Bright phase: Ni (or Co); Light gray phase: NiO (or CoO); dark gray phase: YSZ; dark phase: pore

**Figure 2.** TEM images for a NiO/YSZ (a) and Ni/YSZ (b) samples.

**Figure 3.** Loading/unloading evolution for Co-YSZ at 100nm of penetration depth.

**Figure 4.** Hardness evolution for each phase present in: (a) NiO-YSZ; (b) CoO-YSZ, (c) Ni-YSZ, and (d) Co-YSZ at 100nm of indentation depth.

**Figure 5.** Young's modulus evolution for each phase present in: (a) NiO-YSZ; (b) CoO-YSZ, (c) Ni-YSZ, and (d) Co-YSZ at 100nm of indentation depth.

**Figure 6.** Hardness evolution for each sample performed at 2000nm of indentation depth.

**Figure 7.** Young's modulus evolution for each sample performed at 2000nm of indentation depth.

**Figure 8.** AFM-error micrographs of residual imprints performed at 100 nm of indentation depth in the CoO-YSZ. Inset 1: Magnification of a YSZ grain with several imprints.

**Figure 9.** Topographic image for an YSZ-grain performed in Co-YSZ samples. Innset 1: Magnification of one of the residual imprints.

**Figure 10.** AFM-topography image of residual imprint performed at 2000nm of indentation depth for (a) Co-YSZ and (b) CoO-YSZ.

## Table Captions

**Table 1.** Composition analysed by image analysis (vol%) for the NiO-YSZ and CoO-YSZ eutectics, and also for the Ni-YSZ and Co-YSZ cermets

| **NiO-YSZ** | | | **CoO-YSZ** | | |
|---|---|---|---|---|---|
| **NiO (or Ni)** | **YSZ** | **pores** | **CoO (or Co)** | **% YSZ** | **pores** |
| 56.5 ± 1.7 | 43.5 ± 1.7 | - | 61.0 ± 1.5 | 39.0 ± 1.5 | - |
| **Ni-YSZ** | | | **Co-YSZ** | | |
| 33.1± 0.7 | 43.5 ± 1.7 | 23.4 ± 0.7 | 34.8 ± 0.9 | 39.0 ± 1.5 | 26.2 ± 0.6 |

**Table 2.** *H* and *E* values for NiO-YSZ, CoO-YSZ, Ni-YSZ and Co-YSZ for indentation depths of 100 and 2000nm.

| **Sample** | **Phase** | ***h* = 100 nm** | | ***h* = 2000 nm** | |
|---|---|---|---|---|---|
| | | ***H* (GPa)** | ***E* (GPa)** | ***H* (GPa)** | ***E* (GPa)** |
| **Co-YSZ** | **Co** | 3.9± 0.2 | 102 ± 2 | - | - |
| | **YSZ** | 16.9 ± 0.8 | 179 ± 5 | - | - |
| | **Co-YSZ** | 9.4 ± 0.4 | 159 ± 3 | 5.9 ± 0.6 | 60 ± 2 |
| **Ni-YSZ** | **Ni** | 3.7 ± 0.3 | 65 ± 4 | - | - |
| | **YSZ** | 15.4 ± 0.2 | 180 ± 5 | - | - |
| | **Ni-YSZ** | 6.9 ± 0.4 | 110 ± 3 | 1.0 ± 0.1 | 20 ± 1 |
| **CoO-YSZ** | **CoO** | 5.4 ± 0.2 | 100 ± 2 | - | - |
| | **YSZ** | 12.5 ± 0.2 | 190 ± 5 | - | - |
| | **CoO-YSZ** | 8.8 ± 0.2 | 165 ± 4 | 8.5 ± 0.5 | 185 ± 7 |
| **NiO-YSZ** | **NiO** | 9.5 ± 0.4 | 215 ± 3 | - | - |
| | **YSZ** | 17.5 ± 0.4 | 220 ± 5 | - | - |
| | **NiO-YSZ** | 13.8 ± 0.2 | 219 ± 4 | 12.6 ± 0.3 | 215 ± 4 |

**Table 3.** Bulk E-values for the component phases taken from literature

| | YSZ [11] | NiO | Ni | CoO | Co |
|---|---|---|---|---|---|
| E(GPa) | 220 | 220 | 220 | 170 | 209 |

**Table 4.** Theoretical E-values of the eutectics and porous cermets (see text)

| | |
|---|---|
| CoO-YSZ | 189.5-186.5 |

| | |
|---|---|
| NiO-YSZ | 220 |
| Ni-YSZ | 129.3 |
| Co-YSZ | 101.8 |

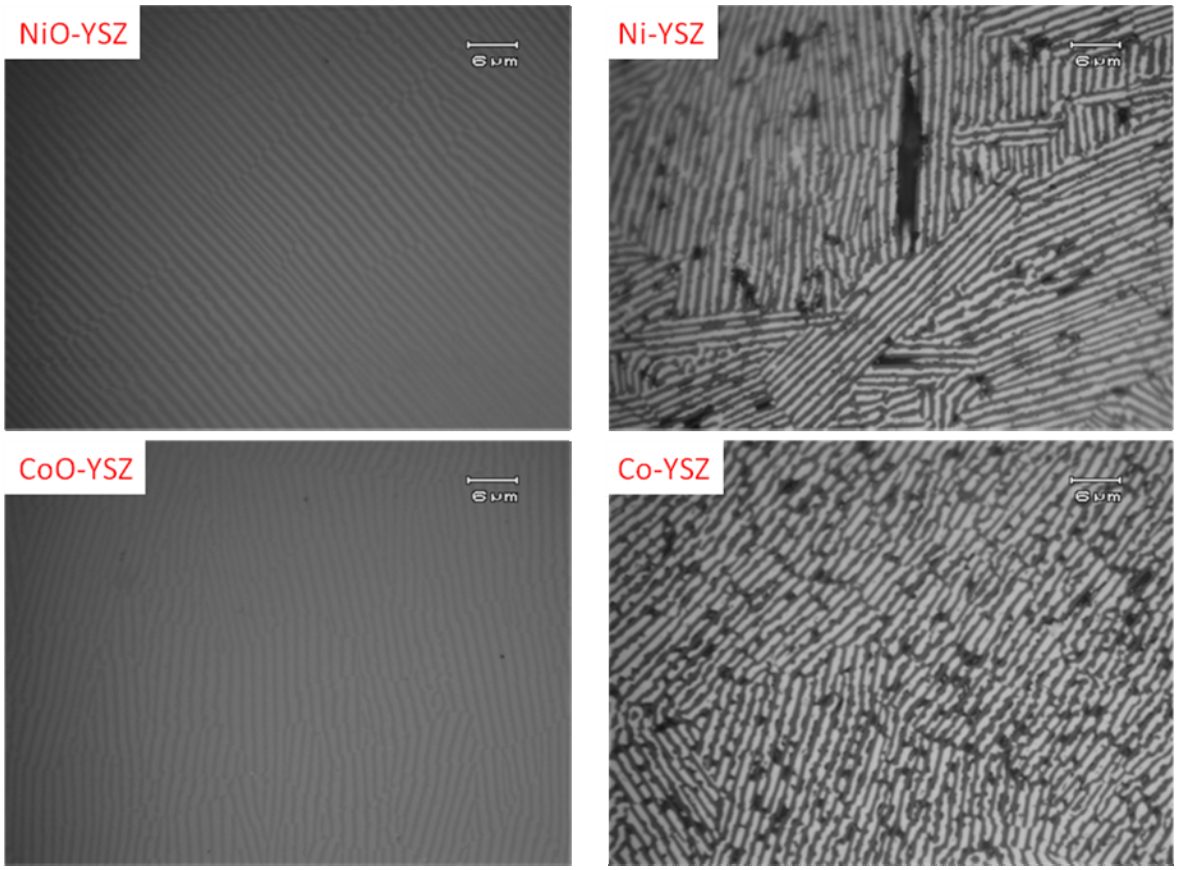

**Figure 1**

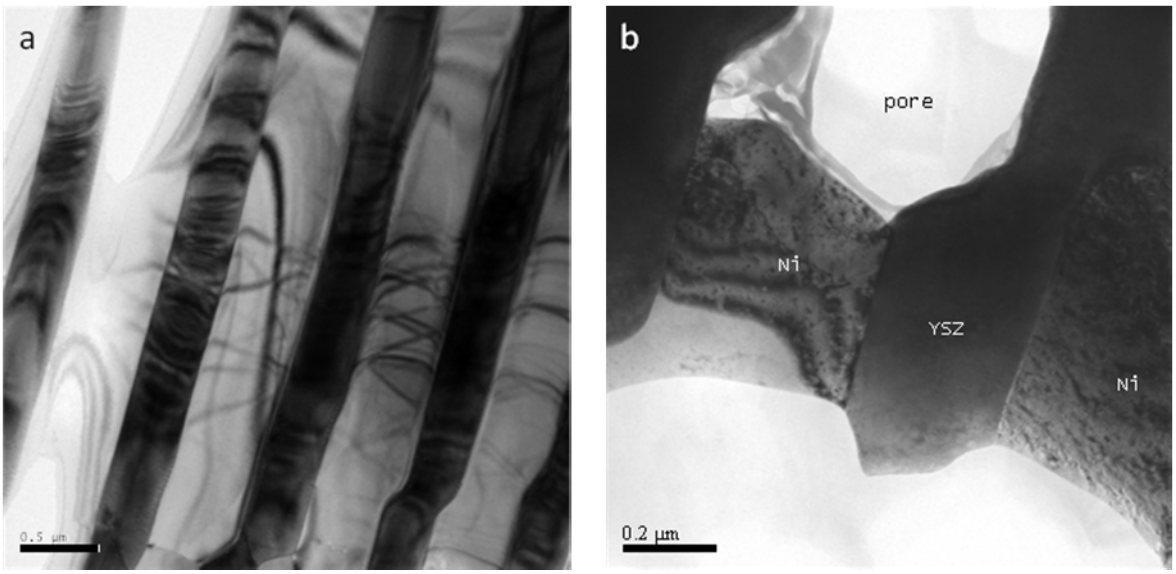


**Figure 2**

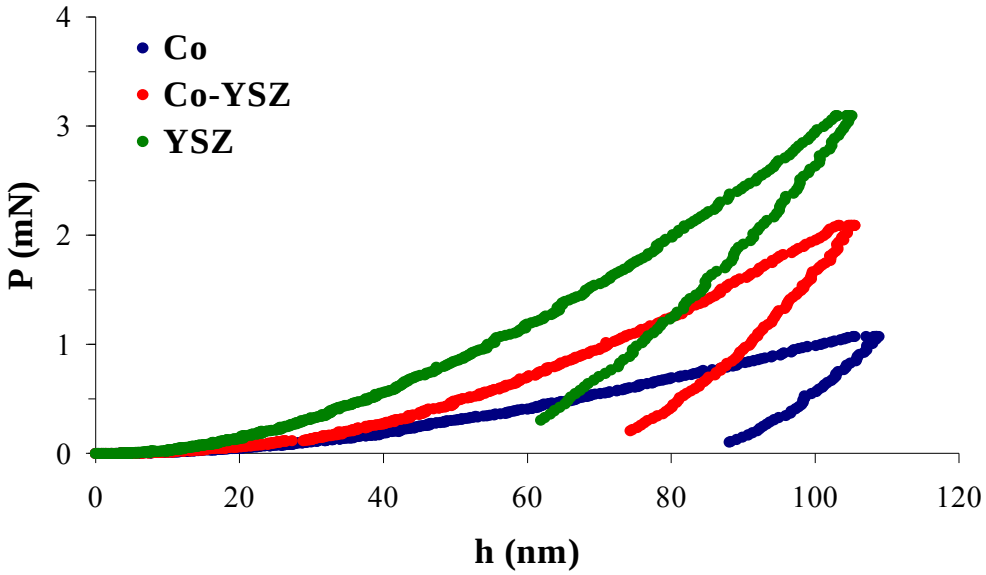


**Figure 3**

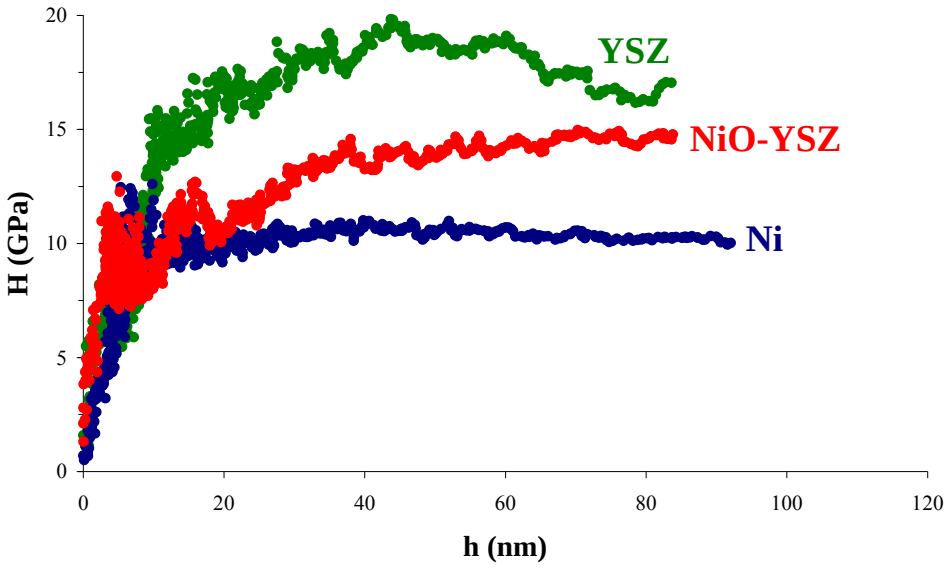


**Figure 4a Esto sería NiO no?**

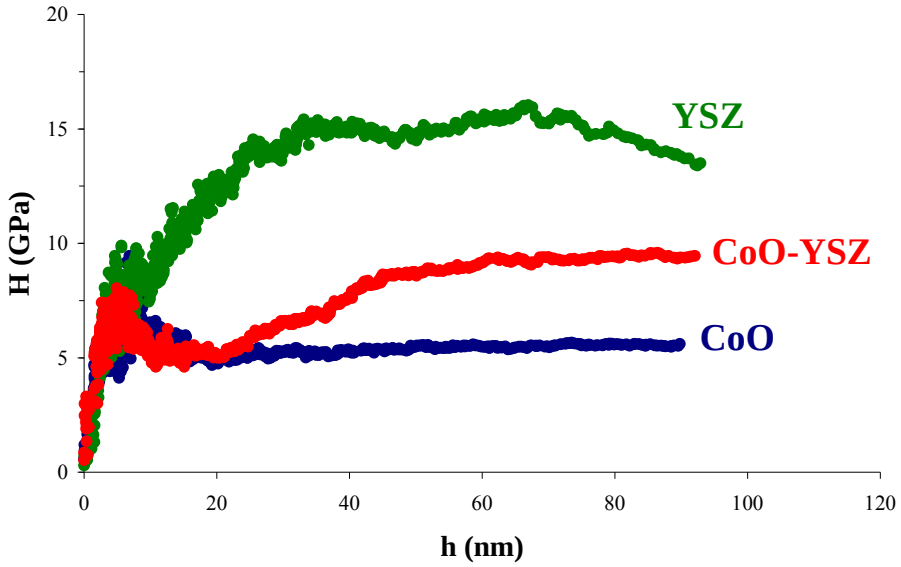


**Figure 4b**

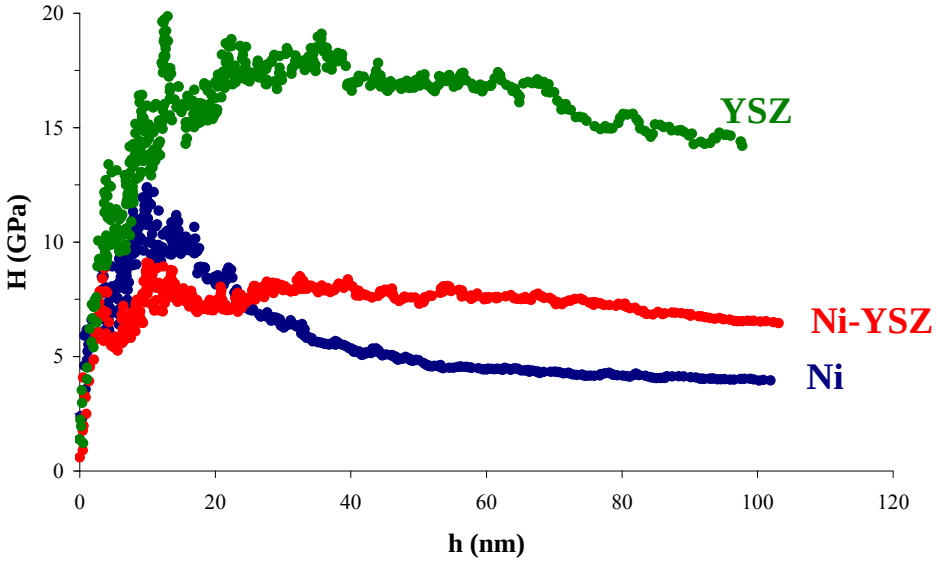


**Figure 4c**

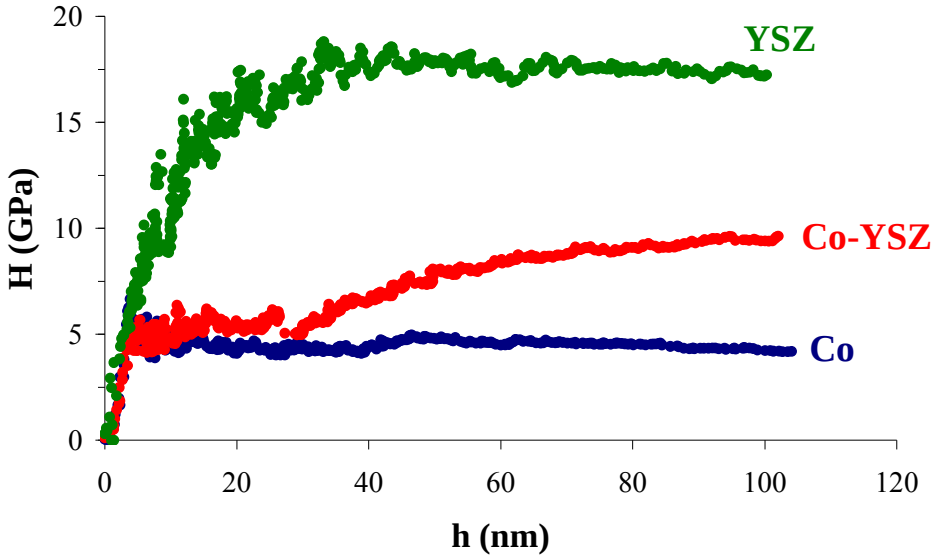


**Figure 4d**

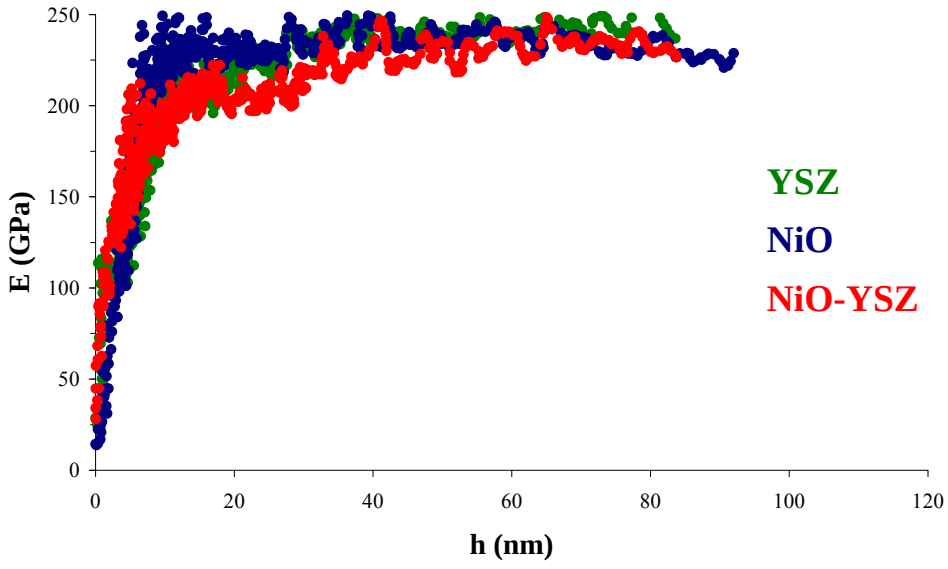


**Figure 5a**

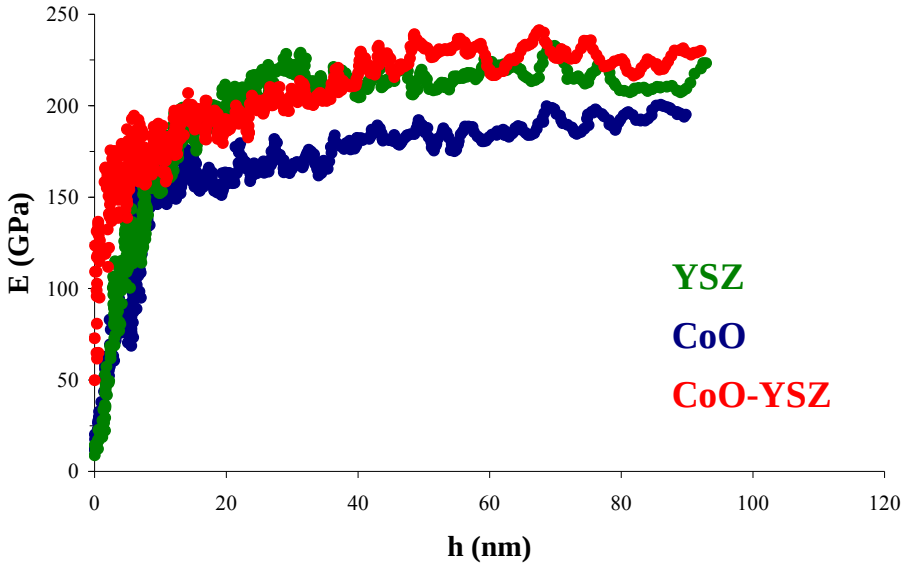


**Figure 5b**

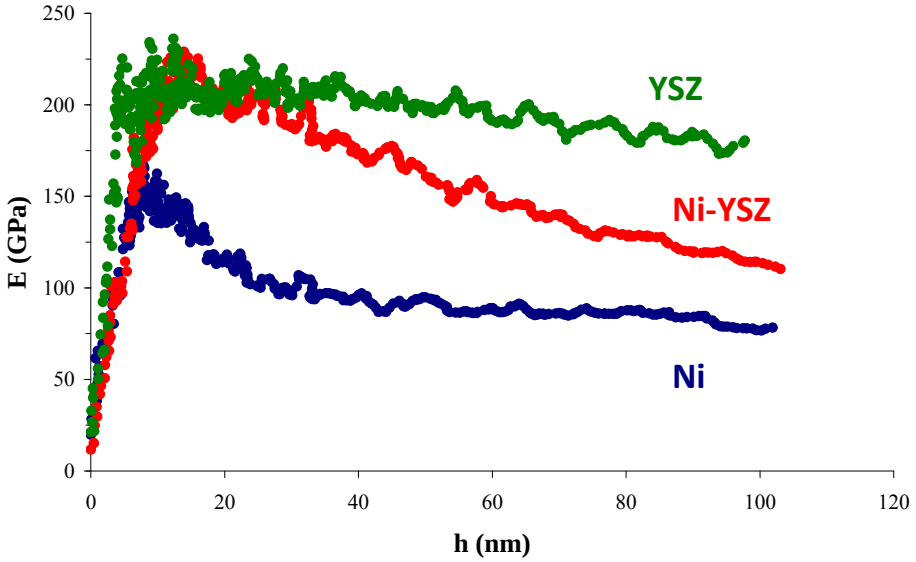


**Figure 5c**

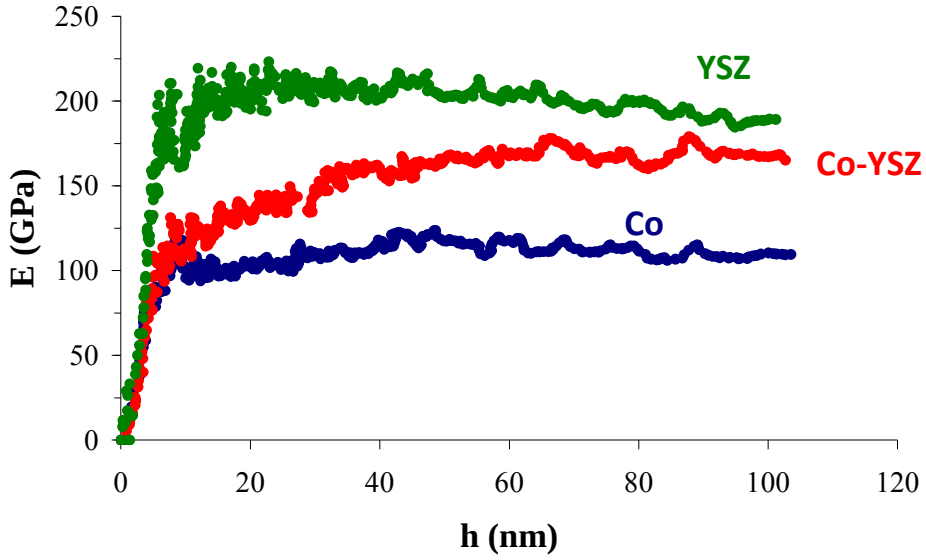


**Figure 5d**

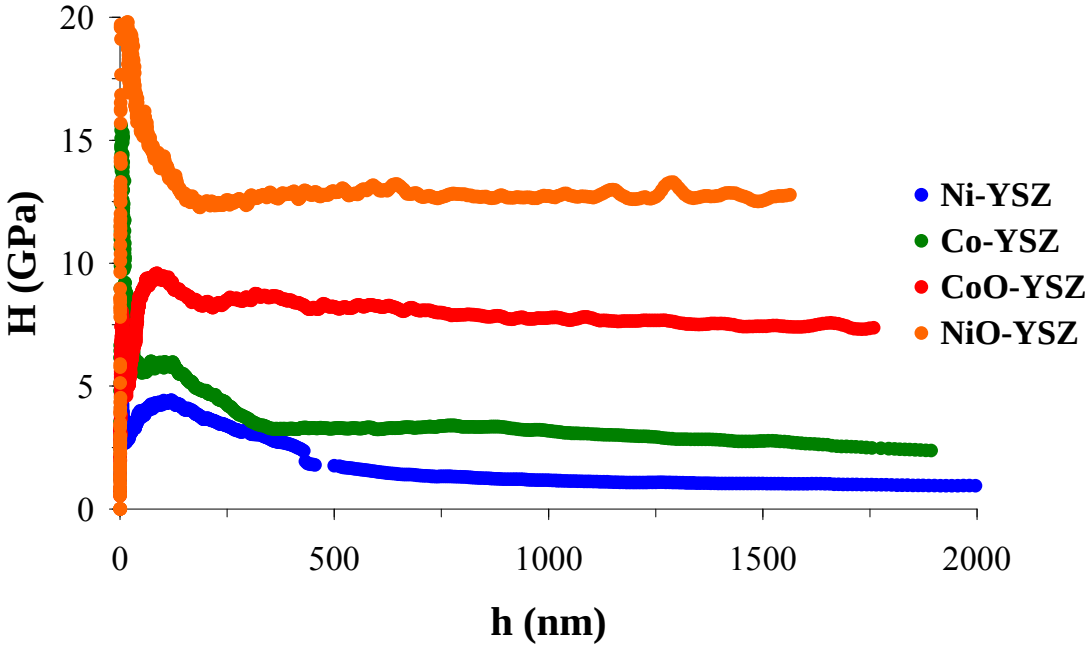


**Figure 6**

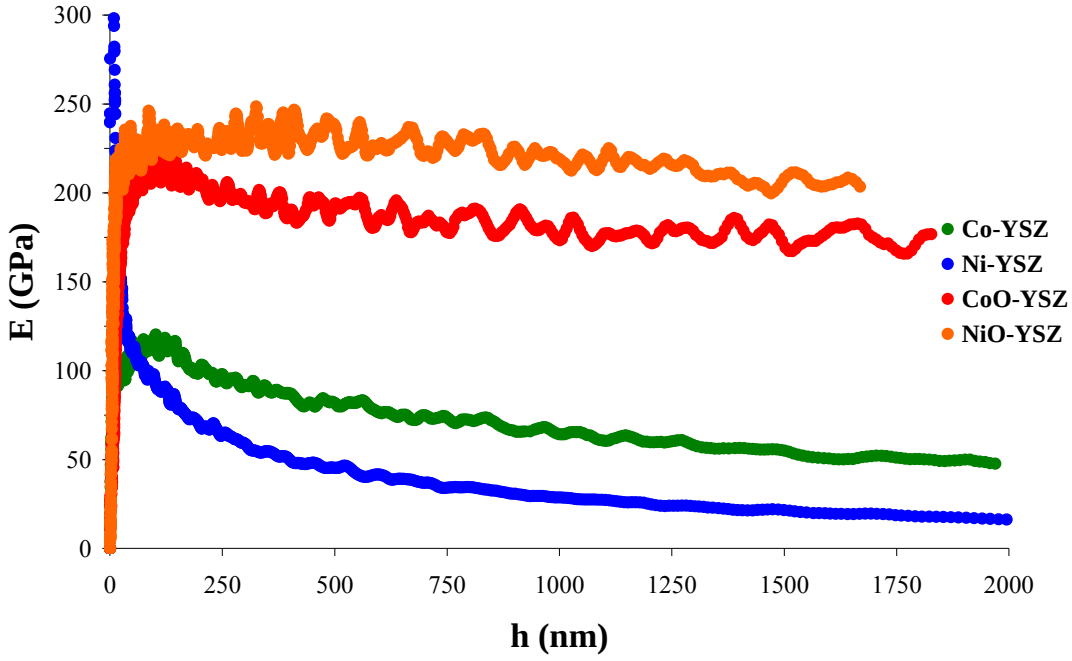
E (GPa)
300
250
200
150
100
50
0
0
250
500
750
1000
1250
1500
1750
2000
h (nm)
Co-YSZ
Ni-YSZ
CoO-YSZ
NiO-YSZ

**Figure 7**

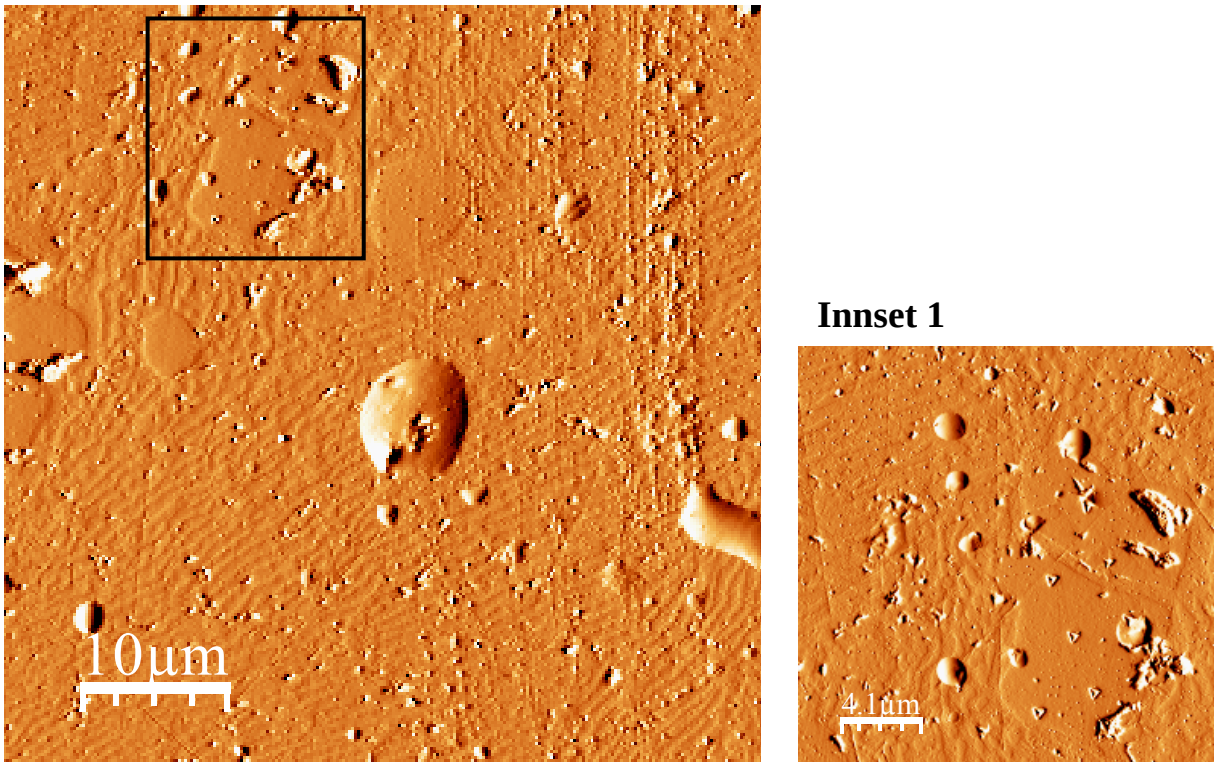


**Figure 8**

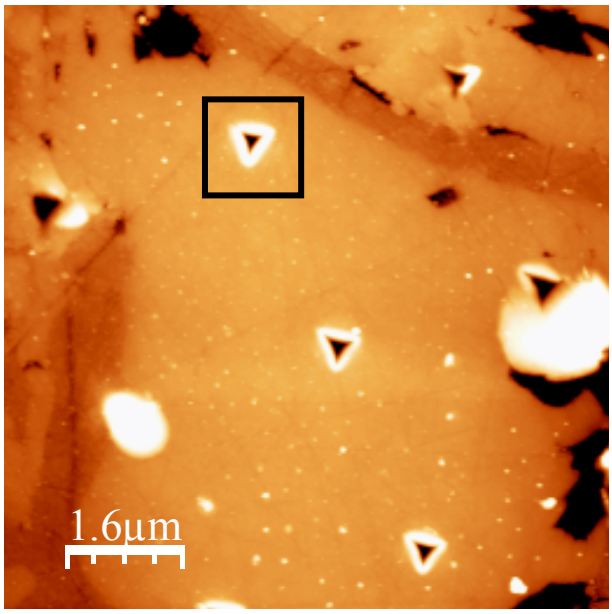


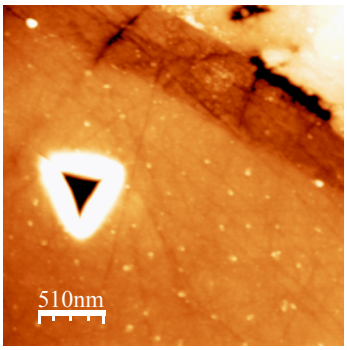


**Innset 1**

**Figure 9**

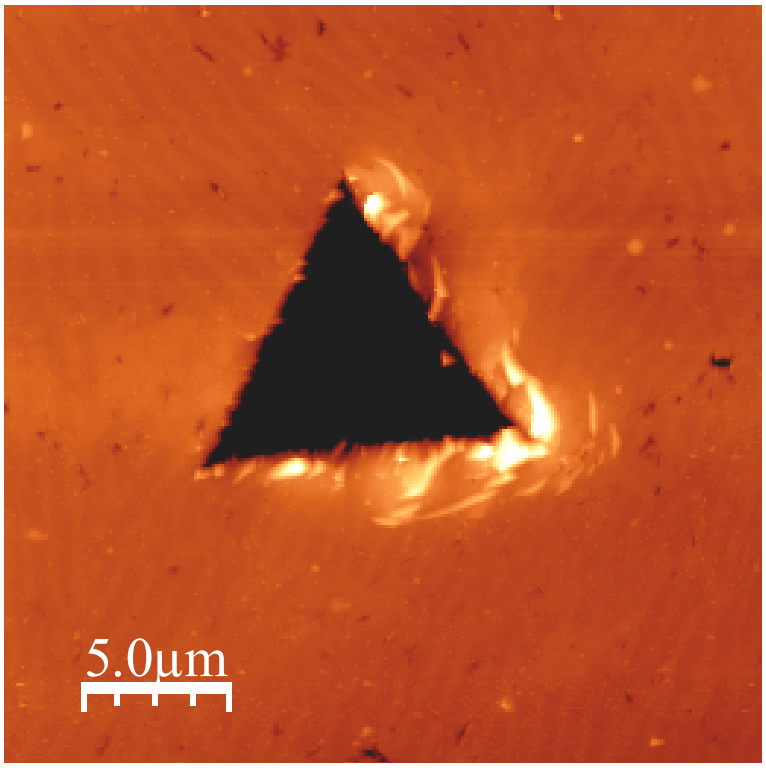


**Figure 10a**

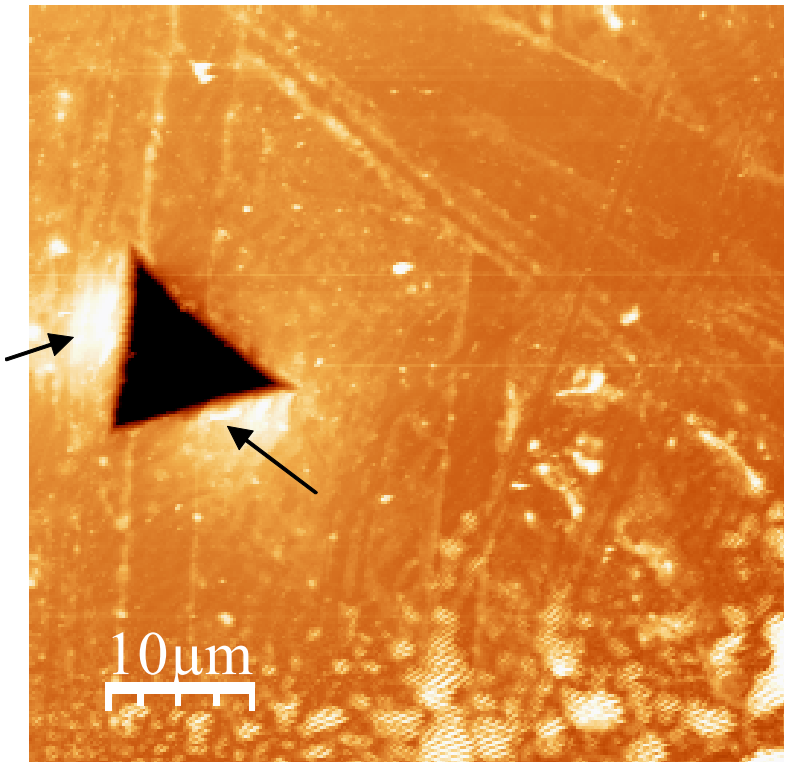


**Figure 10b**